Acta of Bioengineering and Biomechanics
Vol. 25, No. 3, 2023

Original paper
DOI: 10.37190/ABB-02318-2023-03

Biodegradable scaffolds for bone defect treatment

MAGDALENA ANTONOWICZ[1]*, KAROLINA BRZEZIŃSKA[2], WITOLD WALKE[1], ANNA TARATUTA[1], MATEUSZ PAWLIK[3]

[1] Department of Biomaterials and Medical Devices Engineering, Faculty of Biomedical Engineering, Silesian University of Technology, Zabrze, Poland.
[2] SKN SYNERGIA, Department of Biomaterials and Medical Devices Engineering, Faculty of Biomedical Engineering, Silesian Technical University, Zabrze, Poland.
[3] CABIOMEDE Sp. z o.o., Kielce, Poland.

Purpose: Additive techniques in dog orthopedics has recently emerged as a valuable approach in fabricating individualized implants for receiver-specific needs. The scaffolds made by 3D printing are used to replaces bones damaged by injuries sustained in accidents, tumour resections and defects resulting from disease, e.g., osteoporosis. In this way, the growth and reconstruction of bone defects structure can be promoted. These implants should have the right properties to ensure the right conditions for bone fusion. It is also important to determine the time of degradation, which is associated with a significant loss of mechanical properties. *Methods*: Polylactic acid (PLA) scaffolds with different dimensions were fabricated via fused deposition modeling (FDM) by CABIOMEDE for bone tissue reconstruction in veterinary application. During the research, the mechanical properties and impact of the soaking process in Ringer's solution for 1, 3, 6 months and steam sterilization for 1, 2, 3 cycles of the scaffolds were assessed. The static compression and three-point bending tests, material wettability, and macro and microscopic observations were carried out. *Results*: Compressive test results indicated that PLA scaffolds showed elastic–plastics deformation in longitudinal and transverse directions. The compressive strength of the scaffold in initial state were R_{cw} = 5–6 MPa in the longitudinal direction and R_{cp} = 0.33–1 MPa in the transverse direction, depending on size. The flexular strength of the scaffolds were R_g = 348–865 MPa, depending of size. The soaking and steam sterilization process increased the elastic modulus of the material and decreased the flexural strength. Hydrolytic degradation initiated by exposure to Ringer's solution resulted in a change in structure from amorphous to semicrystalline. This indicates partial dissolution of the amorphous phase and thus, an increase in the percentage of the crystalline phase, which caused the material to become brittle. Progressive degradation resulted in brittle fracture of the material, as can be observed in implants after 6 months of soaking. *Conclusions*: The mechanical properties of the PLA scaffolds were close to the properties of cancellous bone. The PLA scaffolds can be anticipated as promising scaffold biomaterials for bone tissue engineering applications by virtue of their bone mimicking porous structure and good mechanical properties.

Key words: *3D printing, bone defect, scaffold, polylactic acid (PLA), veterinary medicine*

1. Introduction

Many owners treat their dogs as members of the family, so when their pets' health deteriorates, they visit the veterinarian immediately. The most common cause of emergency visits of the dogs to veterinarians are bone fractures. They predominate among injuries to the musculoskeletal system, which can be caused by many factors. The most common of injuries are due to traffic accidents [17], [33], fighting with other animals, falls from heights and intentional human actions. Injuries occur regardless of age. Femur shaft fractures often are the result of genetic defects that only become apparent when the animal is growing, breeds or has size-eloping bone tumor. Osteochondrosis is one of the developmental disorders of the skeletal system in dogs, the development of which can result in the formation of cysts. They are most often located in the epiphyses of the long bones, the ulna and the radius. At

* Corresponding author: Magdalena Antonowicz, Department of Biomaterials and Medical Devices Engineering, Faculty of Biomedical Engineering, Silesian University of Technology, Zabrze, Poland, e-mail: magdalena.antonowicz@polsl.pl
Received: September 27th, 2023
Accepted for publication: December 12th, 2023

the site of cyst formation, the bone is weakened, which may result in pathological fracture [31]. Another skeletal disorder diagnosed in dogs is asynchronous forearm bone growth. It manifests itself as a deformation of the long axis of the limb in the area of the carpal bone and the distal epiphysis of the radius or elbow, shortening of the forearm length, and lameness [12]. Among the most commonly diagnosed tumors that affect the canine skeletal system are osteosarcomas, accounting for approximately 85–98% of primary bone tumors [25]. Lesions are most often located in the long bones of the limbs, where the risk of developing them is approximately four times higher than in the bones of the axial skeleton. The second most common primary neoplastic lesions are chondrosarcomas, which account for 5–13% of oncologically treated dogs [5], [26]. Injuries and musculoskeletal conditions in animals require surgical intervention and external immobilization. The use of metal implants carries several possible complications, such as allergic reactions or reoperations performed to remove the implant. On the other hand, the use of a brace makes it difficult to move and also disturbs animals, so they try to get rid of it (often causing difficulties in wound healing). Therefore, the search for methods to eliminate the placement of metal implants and reduce the time of use of total external immobilization has been the subject of plentiful research for years. The dynamic development of veterinary medicine and modern manufacturing techniques allows for the use of bone implants manufactured through additive techniques [16]. Additive techniques in dog orthopedics has recently emerged as a valuable approach in fabricating individualized implants for receiver-specific needs. Additive technologies, also known as 3D printing, involve the creation of physical models, previously designed in CAD systems or obtained by reverse engineering [11]. The process of creating a 3D model takes place layer by layer and, depending on the fabrication technique and the polymer material used, the main techniques used in canine orthopaedics are stereolithography (SLA) and fused deposition modelling (FDM). The SLA method involves curing the liquid resin contained in the workspace. The curing process is made possible by photopolymerisation, performed by a computer-serrated laser. Models made using SLA technology are characterised by high detail resolution and accuracy (the smallest models can reach 50–200 μm). The SLA technology using epoxy resin has been used to produce pre-operative 3D biomodels [6], [13]. On the other hand, the FDM method involves applying a head of molten material, working in the x and y axes. The downward movement of the table along the z-axis creates space for the next layer. The head first creates the contour of the layer and then creates the filling, the type of which is defined in the printer software. The most common materials used in this technology are ABS, PLA and PA12. ABS was also used for preoperative planning to produce a 3D model [3]. With PLA, 3D models of two adult dogs with antebrachial limb deformity [15] and adult golden retriever dog with angular limb deformity [14] were obtained. However, all of the above-mentioned applications relate to the production of preoperative models. The use of additive techniques is increasingly being found in the innovative solution of implants made of biodegradable polymers that serve as a scaffold which can promote growth and reconstruction of bone structure. Scaffold implants are used to replace bones damaged by injuries sustained in mishaps, tumor resections or defects resulting from diseases. FDM 3D printing technology, makes it possible to the control internal porosity, pore size and combined structure of biomaterials. Mainly PLA [1], [9], but also PLA-based composites [19], [32] have found applications in tissue engineering. Currently, the most common implants in veterinary medicine are made of titanium alloys. While effective, these implants' mechanical properties and, in some cases, need of additional surgical procedure for removal, especially in younger animals, can be a significant drawback. In contrast, PLA and its blends, although used primarily for Tibial Tuberosity Advancement procedures, offer a resorbable alternative, eliminating the need for implant removal and reducing the overall stress and risk to the animal.

Scaffolds should have the right properties to ensure the proper conditions for bone fusion. A key issue that determines the success of treatment is the geometric form of the implant and its porosity. In the case of polymer implants, it is also important to determine the degradation time, which is associated with a significant loss of mechanical properties [7]. Among other things, the forces acting on the implants are the main criterion for selecting implant properties. The forces that occur in the body can be divided into internal and external forces. Internal forces include continuous nature, such as those developed by muscles, that are transferred to bones through tendons [4]. The consequence of prolonged exposure to these forces is overloading, resulting in the diagnosis of joint disorders that are most often observed in overweight dogs, as body weight puts additional stress on the skeletal system. External forces acting on the musculoskeletal system usually occur suddenly and their values exceed the forces generated during the animal's normal activity, resulting in bone fractures. Thus, the effectiveness of their use depends on the design itself and the

properties of the material from which scaffolds are made. The surface of the implant should ensure the adhesion and proliferation of bone tissue cells, while the scaffold should serve a supportive function until the bone is rebuilt and proliferated. Therefore, it is important to determine their mechanical properties depending on the function performed, the parameters of the preparation of the structure and the condition of the surface. The implant should be able to carry the loads generated in the limb during the initial healing phase, when the bone is too weak, even if there is a momentary increase in load, such as a total load on the limb when tripping or jumping. The gradual loss of mechanical properties should be temporally correlated with the ability of the growing bone tissue at the defect site to carry the load [2]. A key innovation of our PLA implants is a possibility of easy incorporation of bone growth inhibitors like hydroxyapatite in a gel form, platelet-rich plasma gels or a gels with stem cells which can be induced into the internal porosity of the cylinders. This feature not only aids bone regeneration but also aligns with the natural healing process, enhancing the implant's effectiveness and integration with the animal's bone structure.

The purpose of this study was to determine the mechanical properties of polymeric implants used in veterinary medicine produced by incremental technologies and the effect of degradation on their change. Polylactide (PLA) implants have been manufactured by CABIOMEDE in a selection of dimensions which make them possible to be used in bone defects both for small and large dogs.

2. Materials and methods

2.1. 3D printing of PLA implants

CABIOMEDE's veterinary implants (Fig. 1) made from Evonik's polylactide (PLA) using FDM printing technology on CABIOMEDE's proprietary machine were studied. Machine used for scaffolds manufacturing was CABIOMEDE own modification based on open-source Prusa MK3S developed with full metal hot end, active heated chamber and modified layer cooling system. G-code consisting printing parameters (nozzle temperature of 215 °C, bed temperature of 60 °C) and machine paths were developed using previously developed Python script. The layer thickness was 0.1 mm and the diameter of the printing nozzle was 0.4 mm. The detailed construction and printing algorithm was proprietary to CABIOMEDE. The dimensions of the tested implants depend on the size of bone defect and the breed of dog (Table 1).

Table 1. Dimensions of implants

Group		I	II	III	IV	V	VI	VII	VIII	Plate
Dimension [mm]	D	6	12	18	24	6	12	18	24	20
	H	12	24	36	18	80	80	80	80	50
	B	–	–	–	–	–	–	–	–	5

The test material consisted of cylindrical specimens used to determine mechanical properties during static compression and bending tests, while rectangular plates were prepared to test the wettability and surface energy of the material (Fig. 2). For each test series, five samples were prepared. To evaluate the mechanical properties of the implants after sterilization,

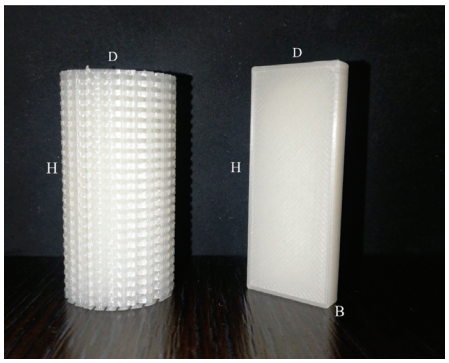

Fig. 2. Geometric form and dimensions of the samples

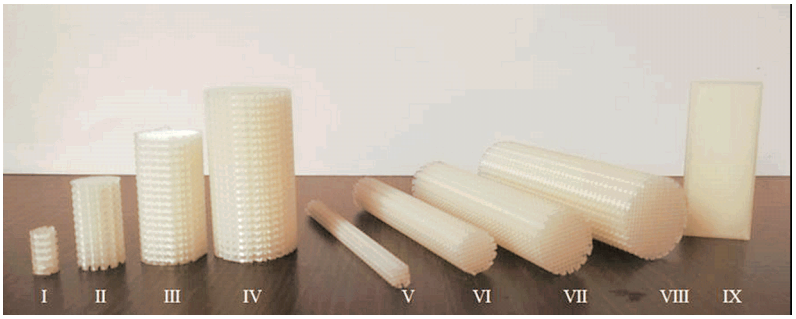

Fig. 1. Implants by CABIOMEDE

they were packaged in paper-foil sleeves, and then steam sterilization was carried out at 121 °C, at 112 KPa using a SUN Class B 18L autoclave. The process was carried out in 1 (PS_1), 2 (PS_2), and 3 cycles (PS_3), 20 min each, respectively.

2.2. *In vitro* tests

In order to assess the biodegradability of the implants and strength properties, implants were exposed for one (R1), three (R3) and six (R6) months in Ringer's solution simulating real conditions in the dog's body. The samples were placed in a thermal cycler at 38 ± 1 °C. After simulating the tissue environment in Ringer solution, pH = 6.5 (8.6 g of NaCl, 0.3 g of KCl, 0.33 g of $CaCl_2$, 1000 dm^3 of water), the samples were subjected to a drying process at 23 ± 1 °C. The weight of the implants was then measured using a RADWAG electronic laboratory balance. Before the study, the weight of the implants was measured at the beginning of the study and after exposure to Ringer's solution.

2.3. Mechanical properties

Static uniaxial compression testing was performed according to the recommendations of PN-EN ISO 604:2006 [21] at a constant speed of v = 1 mm/min on an MTS Criterion testing machine in both longitudinal and transverse directions. The tests were performed at room temperature. Specimens of 6 × 12, 12 × 24, 18 × 36, and 24 × 48 [mm] (groups I–IV) were tested in the initial state, for each sterilization cycle, as well as exposure to Ringer's solution. Five samples were tested for each variant. The static three-point bending test was carried out according to the recommendations of PN-EN ISO 178: 2019 [20] at a constant speed of v = 5 mm/min at room temperature on an MTS Criterion testing machine. The distance between the crossbars was l = 52 mm and the diameter of the rollers on which the specimen was placed was d = 5 mm. The test was carried out for implants with a length of L = 80 mm and diameters D of 6, 12, 18, and 24 [mm], respectively, (groups V–VIII) in the initial state, after each sterilization cycle and exposure to Ringer's solution. The bending test was performed on 5 samples of each variant.

2.4. Surface morphology

Observations were made on a Leica optical microscope at 50×, 100×, 500× and 1000× magnifications. Areas of delamination or cracks in the print path as well as samples in the initial state were observed. Scanning electron microscopy (SEM), TESCAN VEGA 4 under low vacuum conditions at 15 keV using a secondary electron detector SE was carried out. The observations were made for the initial state and the implants after static compression and bending tests.

2.5. Chemical composition test

Qualitative analysis of the chemical composition was performed using a scanning electron microscope equipped with Energy dispersive X-ray spectroscopy (EDS) equipment. The study was carried out at 15 keV. Qualitative analysis was performed for the implant at baseline and after exposure to a simulated tissue environment to identify the precipitate deposition from the Ringer's solution.

2.6. Wettability tests of PLA surfaces

To determine the surface wettability of the selected samples, wetting angle measurements were carried out using the sitting drop method, and surface free energy (SEP) measurements were carried out using the Owens –Went method. Young's equation was used to determine the surface energy. Measurements were made with demineralized water (w) and diiodomethane (d) at room temperature T = 23 ± 1 °C. Polar and dispersion components for distilled water were γ_{sp} = 51.0 [mJ/m^2] and γ_{sd} = 21.8 [mJ/m^2] and for diiodomethane: γ_{sp} = 6.7 [mJ/m^2] and γ_{sd} = 44.1 [mJ/m^2]. Measurements were made on a test stand, which consisted of a SURFTENS UNIVERSAL goniometer from OEG and SURFTENS 4.5 software. Five drops of distilled water and 1 mm^3 of diiodomethane were applied successively to the surface of each sample. Angle measurements were taken 15 seconds after placing the drop on the test material to stabilize it. One measurement was conducted for 60 seconds, with a sampling frequency of 1 Hz. The average values of the wetting angle and surface free energy were determined from the tests.

2.7. Statistical analysis

In the study, for the mechanical research method, the sample populations were presented as means with standard deviation (SD) for quantitative data. In order to determine the significance of differences for $p < 0.05$, the one-way analysis of variance (ANOVA) for the ob-

tained results were used. Each test was performed on five different scaffold.

3. Results

3.1. *In vitro* testes

The results of the weight measurements are shown in Fig. 3a. An increase in the weight of the samples after one and three months of soaking was observed as a result of salt deposition from the Ringer solution. Further exposure to Ringer solution resulted in a decrease in implant weight of the implants due to the detachment of the outer layers of the specimen, Fig. 3b.

In group II, after 1-month exposure to Ringer's solution, a decrease in compressive strength was observed (IS_gr_II R_{cw} = 6 MPa, R1_gr_II R_{cw} = 4 MPa), while after 3 months of soaking, the compressive strength of the implants increased compared to baseline (R3_gr_II R_{cw} = 10 MPa). Moreover, the effect of soaked after 1 and 3 months was significant ($p < 0.05$) for the value of mechanical properties for scaffold. For group III and IV samples, 1- and 3-month exposure to Ringer's solution resulted in an increase in compressive strength (R1_gr_III R_{cw} = 9 MPa, R3_gr_III R_{cw} = 10 MPa) compared to baseline (IS_gr_III R_{cw} = 5 MPa) ($p < 0.05$). For all groups of specimens, 6 months of exposure to Ringer's solution resulted in a decrease in longitudinal compressive strength to a value of about 1 MPa. Implants after sterilization, regardless of the group, showed higher compressive strength values (S1_gr_IV

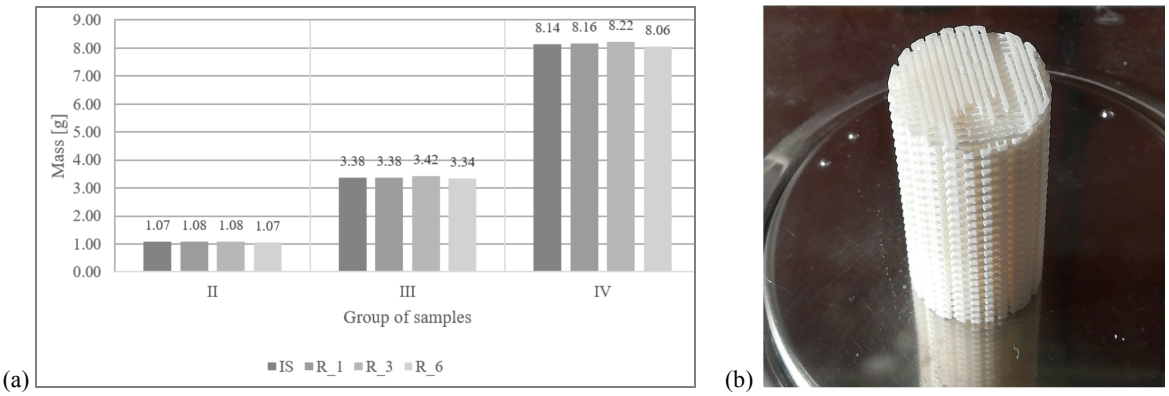

Fig. 3. Implants: (a) weight measurements, (b) breaking off the outer layer

3.2. Mechanical properties

The results of the static compression test in the longitudinal direction are shown in Table 2. The stress–strain relationship is shown in Fig. 4.

R_{cw} = 9 MPa, S2_gr_IV R_{cw} = 8 MPa, S3_gr_IV R_{cw} = 6 MPa) than the baseline condition (IS_gr_IV R_{cw} = 5 MPa) ($p < 0.05$), except for samples after 1 sterilization cycle from group III, where the maximum value of force F_{max} decreased by 1 MPa. The highest value of modulus of elasticity (S3_gr_III E = 502 MPa)

Table 2. Results of the static compression test in the longitudinal direction

	12 × 24 – Group II			18 × 36 – Group III			24 × 48 – Group IV		
	F_{max} [N]	R_{cw} [MPa]	E [MPa]	F_{max} [N]	R_{cw} [MPa]	E [MPa]	F_{max} [N]	R_{cw} [MPa]	E [MPa]
IS	704 ± 166	6 ± 1	476 ± 5	1300 ± 270	5 ± 1	408 ± 6	2160 ± 603	5 ± 1	422 ± 3
R_1	464 ± 25	4 ± 0.2	540 ± 1	2270 ± 220	9 ± 1	439 ± 5	5064 ± 112	11 ± 0.3	121 ± 5
R_3	1155 ± 170	10 ± 2	527 ± 20	2420 ± 230	10 ± 1	425 ± 11	4914 ± 124	11 ± 0.3	455 ± 3
R_6	123 ± 1	1 ± 0.01	48 ± 3	169 ± 85	1 ± 0.3	45 ± 16	277 ± 163	1 ± 0.4	48 ± 13
S_1	1219 ± 195	11 ± 2	534 ± 16	1158 ± 358	5 ± 1	461 ± 12	4206 ± 374	9 ± 0.8	470 ± 16
S_2	1134 ± 156	10 ± 1	594 ± 19	1965 ± 103	8 ± 0.4	489 ± 5	3766 ± 246	8 ± 0.6	495 ± 27
S_3	832 ± 158	7 ± 1	585 ± 4	1759 ± 246	7 ± 1	502 ± 1	2733 ± 416	6 ± 1	500 ± 3

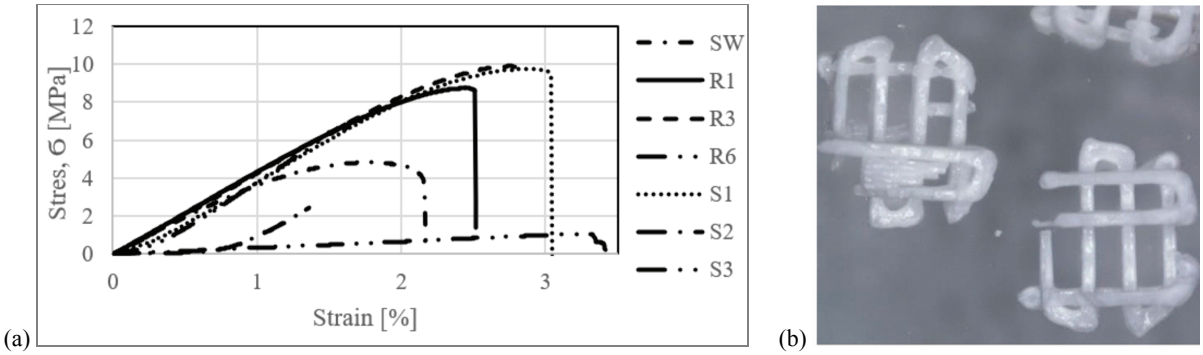

Fig. 4. Results of static uniaxial compression test in the longitudinal direction: (a) stress–strain relationship for samples with dimensions of 18 × 36 mm, (b) implants damaged as a result of degradation (group I)

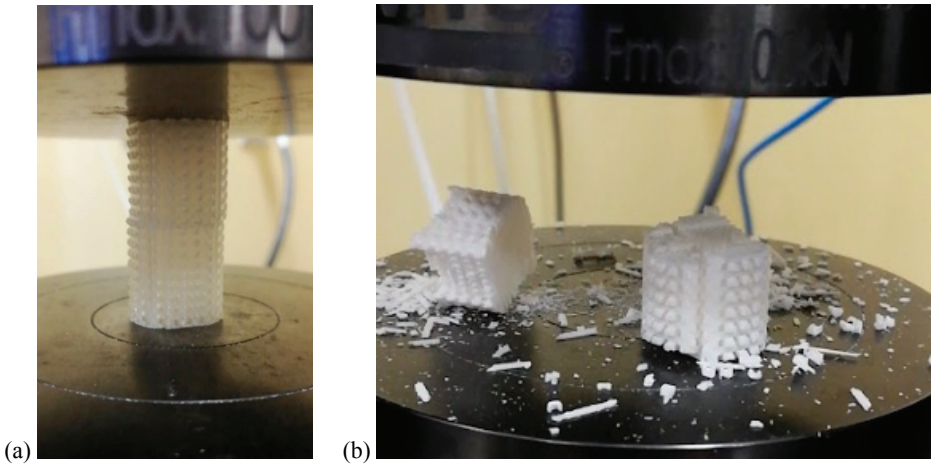

Fig. 5. Samples for static uniaxial compression test in the longitudinal direction: (a) initial condition (IS), (b) after 6 months of exposure to Ringer's solution (R_6)

Table 3. Results of the static compression test in the transverse direction

	12 × 24 – Group II			18 × 36 – Group III			24 × 48 – Group IV		
	F_{max} [N]	R_{cp} [MPa]	E [MPa]	F_{max} [N]	R_{cp} [MPa]	E [MPa]	F_{max} [N]	R_{cp} [MPa]	E [MPa]
IS	310 ± 80	1 ± 0.3	102 ± 6	1850 ± 100	2.8 ± 0.1	60 ± 19	384 ± 171	0.33 ± 0.14	9.3 ± 2
R_1	600 ± 110	2 ± 1.5	104 ± 19	2000 ± 190	3.5 ± 0.2	55 ± 10	2720 ± 268	2.36 ± 0.2	66 ± 12
R_3	480 ± 110	1.65 ± 0.4	73 ± 14	404 ± 300	0.6 ± 0.3	53 ± 8	1150 ± 576	1 ± 0.5	55 ± 9
R_6	40 ± 30	0.1 ± 0.1	13 ± 5	16 ± 11	0.03 ± 0.01	31 ± 5	160 ± 38	0.14 ± 0.03	17 ± 8
S_1	230 ± 90	0.2 ± 0.2	37 ± 19	1288 ± 264	2 ± 0.3	32 ± 6	2360 ± 340	2 ± 0.3	64 ± 2
S_2	180 ± 70	0.3 ± 0.02	60 ± 40	325 ± 86.4	0.5 ± 0.09	46 ± 11	420 ± 342	0.4 ± 0.3	31 ± 13
S_3	70 ± 10	0.3 ± 0.03	14 ± 2	59.3 ± 36.1	0.1 ± 0.04	35 ± 12	62 ± 7	0.05 ± 0.006	19 ± 0.4

($p < 0.05$) is characterized by samples after 3 sterilization cycles, while the lowest value is for samples after 6 months of exposure to Ringer's solution (R6_gr_III $E = 48$ MPa) ($p < 0.05$).

The results for group I (6 × 12 mm) were not included in the analysis due to their miniaturized geometric form. The size of the specimens made it impossible to perform a static compression test due to the small contact area with the grips of the testing machine, especially for specimens that had degraded.

Comparison of the specimen at baseline and after 6-month exposure to Ringer's solution following a compression test in the longitudinal direction (Fig. 5).

The results of the static compression test in the transverse direction are shown in Table 3. The stress–strain relationship is shown in Fig. 6.

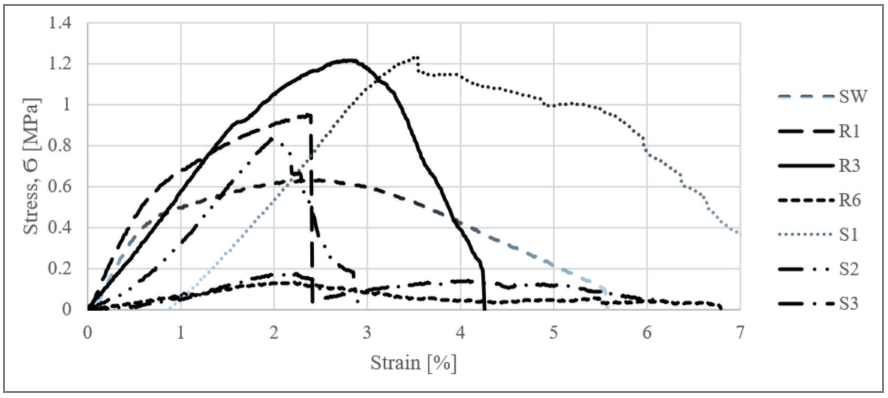

Fig. 6. Static uniaxial compression test in the transverse direction: stress–strain relationship for samples with dimensions of 12 × 24 mm

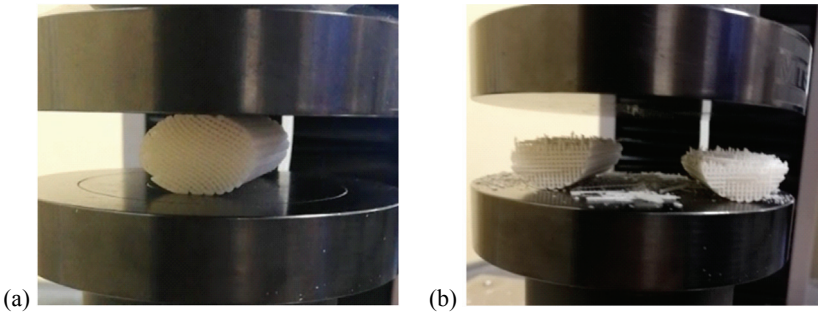

Fig. 7. Samples after static uniaxial bending test in the transverse direction: a) initial condition (IS), b) after 6-month exposure to Ringer's solution (R_6)

Table 4. Results of the three-point bending test

	6 × 80 – Group V			12 × 80 Group VI			18 × 80 Group VII			24 × 80 Group VIII		
	F_{max} [N]	R_g [MPa]	f [mm]	F_{max} [N]	R_g [MPa]	f [mm]	F_{max} [N]	R_g [MPa]	f [mm]	F_{max} [N]	R_g [MPa]	f [mm]
IS	9840 ± 1200	348 ±43	2.105 ± 0.33	97748 ± 14665	865 ± 129	1.4 ± 0.35	186160 ± 26670	732 ± 105	1.8 ± 0.3	350613 ± 140884	775 ± 310	2.7 ± 1.5
R_1	9125 ± 2300	322 ± 80	1.5 ± 0.4	92461 ± 8611	818 ± 76	1.2 ± 0.4	134890 ± 27680	530 ± 109	0.99 ± 0.3	333615 ± 46826	738 ± 103	2 ± 0.8
R_3	4349 ± 900	154 ± 31	0.67 ± 0.11	43675 ± 17123	386 ± 151	0.5 ± 0.2	71690 ± 13020	382 ± 51	0.57 ± 0.06	183621 ± 4776	406 ± 11	1.4 ± 0.06
R_6	2313 ± 1200	81 ± 40	0.26 ± 0.2	796 ± 210	7 ± 1.9	0.2 ± 0.06	880 ± 110	3 ± 4	0.08 ± 0.04	1390 ± 0	6 ± 0	0.2 ± 0
S_1	4875 ± 900	173 ± 31	0.62 ± 0.08	40343 ± 8835	357 ± 78	0.4 ± 0.1	66890 ± 19110	236 ± 75	0.54 ± 0.1	218326 ± 12584	483 ± 28	1.1 ± 0.06
S_2	2513 ± 1300	89 ± 46	0.47 ± 0.42	29830 ± 6172	257 ± 55	0.3 ± 0.06	56790 ± 22530	223 ± 87	0.44 ± 0.2	111971 ± 15162	248 ± 34	0.6 ± 0.07
S_3	2352 ± 600	83 ± 20	0.47 ± 0.27	19206 ± 3359	170 ± 29	0.02 ± 0.03	28310 ± 6220	111 ± 24	0.32 ± 0.1	80263 ± 7982	178 ± 18	0.5 ± 0.07

The highest compressive strength was demonstrated by implants after 1 month of soaking in Ringer's solution (R1_gr_II R_{cp} = 2 MPa, R1_gr_III R_{cp} = 3.5 MPa, R1_gr_IV R_{cp} = 2.4 MPa) ($p < 0.05$). On the other hand, the lowest compressive strength in the transverse direction was found in group II and III implants after 6 months of exposure to Ringer solution (R6_gr_II R_{cp} = 0.1 MPa, R6_gr_III R_{cp} = 0.3 MPa) and in group IV samples after 3 sterilization cycles (S3_gr_IV_ R_{cp} = 0.05 MPa) ($p < 0.05$). In groups II and III, the lowest elastic modulus (E) was recorded for samples after 6 months of soaking in Ringer solution (R6_gr_II E =

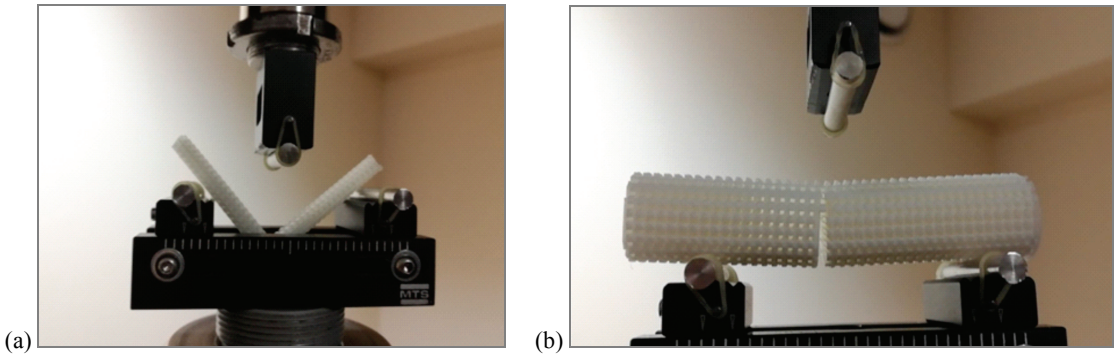

Fig. 8. Samples after static three-point bending test: (a) group VI, (b) group VIII

13 MPa, R6_gr_III E = 31 MPa) while in group IV for samples in the initial state (IS_gr_IV E = 9.3 MPa) ($p < 0.05$).

A comparison of the sample at baseline and after 6 months of exposure to Ringer solution following a longitudinal compression test is shown in Fig. 7.

The results of the static three-point bending test are shown in Table 4, while the samples after the test are shown in Fig. 8.

The highest flexural strength values were obtained for the samples in the initial state in all groups (IS_gr_V R_g = 348 MPa, IS_gr_VI R_g = 865 MPa, IS_gr_VII R_g = 732 MPa, IS_gr_VIII R_g = 775 MPa) ($p < 0.05$). Soaking in Ringer's solution affected the decrease in flexural strength (R_g) in all groups of samples. The lowest flexural strengths are characterized by samples after 6-month exposure to Ringer's solution (R6_gr_V R_g = 81 MPa, R6_gr_VI R_g = 7 MPa, R6_gr_VII R_g = 3 MPa, R6_gr_VIII R_g = 6 MPa) ($p < 0.05$). In contrast, as the number of sterilization cycles increased, the flexural strength decreased (S1_gr_V R_g = 173 MPa, S2_gr_V R_g = 89 MPa, S3_gr_V R_g = 83 MPa) ($p < 0.05$). The highest values of the deflection arrow were recorded for the samples under the initial conditions, while the samples subjected to 6-month exposure to Ringer's solution have the lowest deflection arrow (IS_gr_VIII f = 2.7 mm, IS_gr_VIII f = 0.2 mm) ($p < 0.05$).

3.3. Macroscopic and microscopic evaluation

Macroscopic observations of the surface of the PLA material from which the implants were made showed a change in the color of the implants after exposure to Ringer solution (Fig. 9). Areas of delamination or cracks in the print path were observed. The pore size and the print path is shown in Fig. 9, while the average pore size is shown in Table 5. Observations of the implants after a static compression test are shown in Fig. 10 and after a three-point bending test in Fig. 11.

In the design of the implants in the initial state, after one month of soaking and one sterilization cycle, no cracks were observed but they were deformed – there was a shift in the print paths under load. The largest deformation was observed in the sample after one month of exposure to Ringer's solution, which shows the highest compressive strength in the transverse direction (R_{cp}) in the group. Observations of the

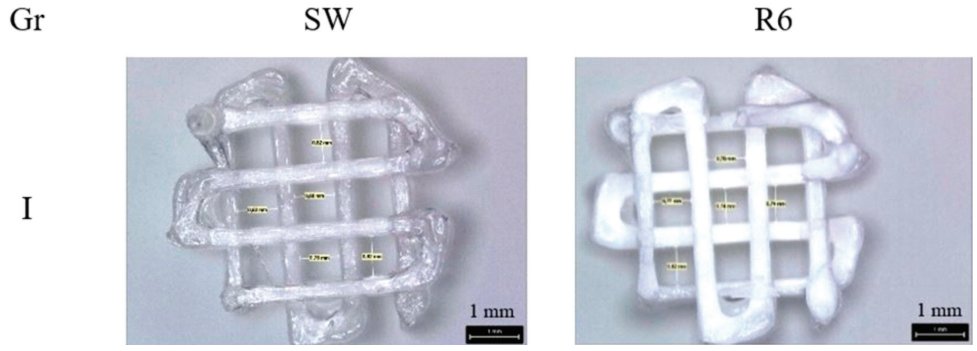

Fig. 9. Measurement of pore size and print path thickness, visible color change of implants exposed to Ringer's solution, mag. 100×

Table 5. Average size of pores and implant printing paths depending on the variant

	Group I		Group II		Group III		Group IV	
	pores	path	pores	path	pores	path	pores	path
IS	0.8	0.4	0.8	0.38	0.8	0.38	0.79	0.39
R_1	0.76	0.38	0.79	0.39	0.8	0.38	0.78	0.38
R_3	0.76	0.37	0.8	0.38	0.8	0.39	0.77	0.39
R_6	0.77	0.39	0.78	0.4	0.78	0.38	0.79	0.39
S_1	0.77	0.37	0.77	0.39	0.8	0.39	0.79	0.39
S_2	0.8	0.38	0.8	0.38	0.8	0.38	0.79	0.39
S_3	0.81	0.38	0.79	0.38	0.8	0.38	0.78	0.39

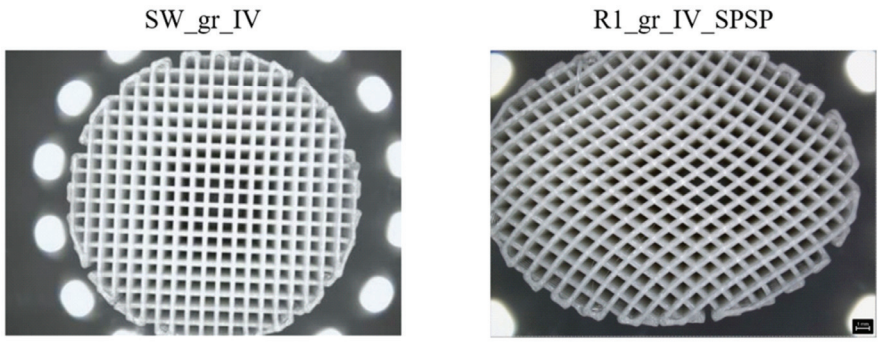

Fig. 10. Samples (group IV) after a static compression test in the transverse direction, mag. 25×

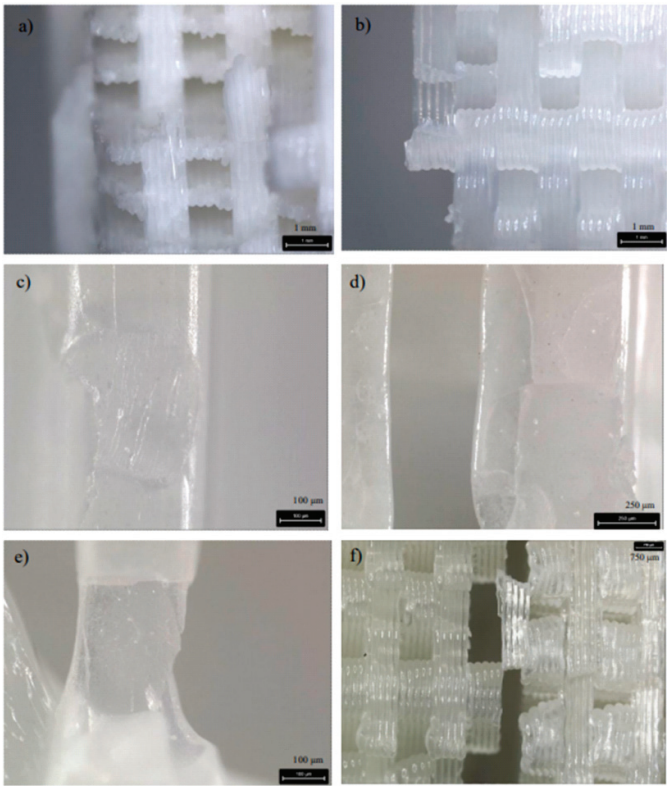

Fig. 11. Damage after the three-point bending test: (a) breakage – R6_gr_III sample, mag. 100×, (b) cracking – S3_gr_IV mag. 100×, (c) path breakage – S3_gr_I mag. 1000×, (d) cracks paths – R6_gr_II mag. 500×, (e) R6_gr_I mag. 1000×, f) IS_gr_VIII mag. 100×

failure points of the samples after the static compression and three-point bending tests are shown in Fig. 11.

Microscopic observations (SEM) of the samples in their initial state after static compression testing are shown in Figs. 12 and 13. In the images, the irregu-

larity of the print paths can be seen as where they are connected.

3.4. Chemical composition test

In Figure 14, a qualitative analysis of the chemical composition of the implant in the initial state (a) and after 6 months of exposure to Ringer's solution (b) is shown. The EDS microanalysis of the implant surface in the initial state in the selected area (Fig. 14a) showed the presence of carbon (55.7%) and oxygen (44.3%). Microscopic observation of the implant exposed to Ringer's solution additionally revealed crystals formed by salt deposition from the Ringer solution (Fig. 14b). Their

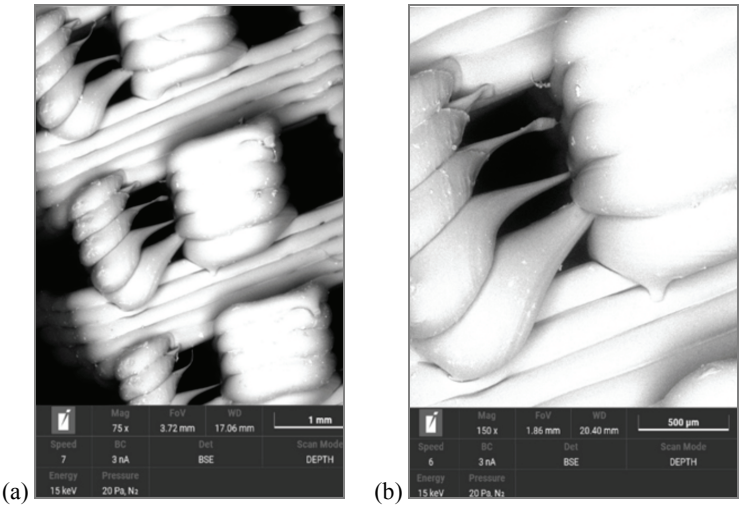

Fig. 12. SEM observation of print paths in the initial state: (a) mag. 75×, (b) mag. 150×

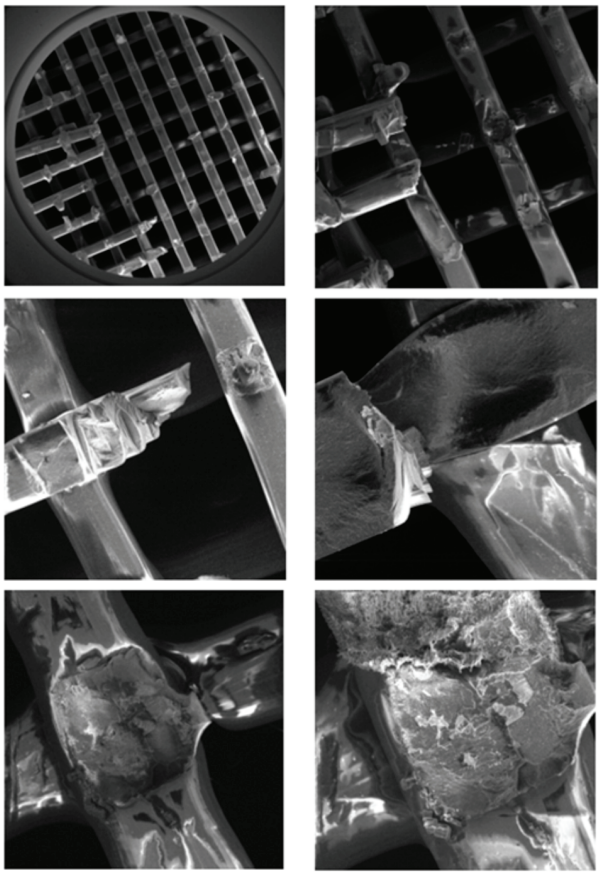

Fig. 13. Microscopic observations of samples after 6-month exposure to Ringer's solution – SEM: (a) mag. 75×, (b) mag. 100×, (c) mag. 150×, (d) mag. 250×, (e) mag. 250×, (f) mag. 300×

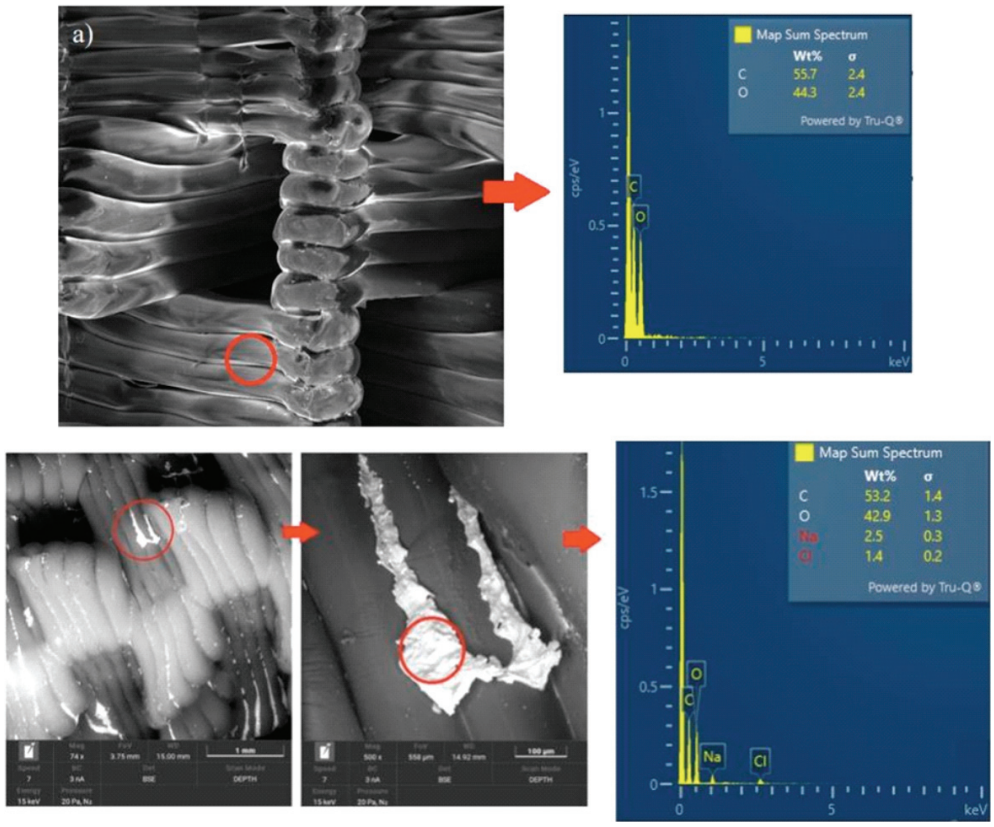

Fig. 14. Basic microanalysis of implant chemical elements:
a) in the initial state, b) after six months of exposure to Ringer's solution

analysis revealed the presence of sodium (2.5%) and chlorine (1.4%).

3.5. PLA surface wettability tests

The results of the wetting angle and surface energy of PLA surfaces are shown in Table 6. Both the implant surface at baseline and after one month of exposure to Ringer solution shows a hydrophilic character (<90°). The soaking process slightly affected the increase in the wetting angle ($p < 0.05$). Hydrophilicity is a desirable feature for tested implants, as it determines the rate of cell adsorption and adhesion, which is particularly important with scaffolds [27], [28].

4. Discussion

The additive techniques in dog orthopedics has recently emerged as a valuable approach in fabricating individualized implants for receiver-specific needs. The scaffolds by FDM methods made of biodegradable PLA materials simulating bone structure and function in physical and chemical properties can promote growth and reconstruction of bone structure. Scaffolds should have sufficient elastic modulus and compressive strength to support bone growth and should be characterised by a 3D pore porous structure, and be able to degrade gradually with new bone growth [2], [32]. Our study introduces 3D printed PLA implants specifically designed for scenarios where biodegradability offers significant advantages. This is par-

Table 6. Results of contact angle and surface energy

Sample	Distilled water	Diiodomethane	γ_s^p [mJ/m^2]	γsd [mJ/m^2]	γS [mJ/m^2]
	Contact angle [θ°]	Contact angle [θ°]			
IS	37.65 ± 2.82	44.29 ± 1.65	42.23 ± 3.50	16.27 ± 1.43	58.50 ± 2.10
R1	46.98 ± 1.65	45.33 ± 1.14	33.55 ± 1.99	18.13 ± 0.94	51.67 ± 1.17

ticularly relevant in young and growing animals (especially near joint regions), as well as in non-load bearing conditions (e.g., skull, or missing bone fragments in bridging plating). The biodegradable nature of PLA avoids the need for a second surgery to remove the implant, which is especially beneficial in growing animals where the dynamics of bone growth are a critical factor. For the proposed PLA scaffolds in different sizes, tests were carried out to meet the mechanical and degradation requirements of load-bearing bone scaffolds. The static compression and three-point bending tests were carried out. In this study, the functional properties of the implants were evaluated in the initial state, as well as after simulating the tissue environment in Ringer solution and after steam sterilization. Compressive strength is an important property of an implant due to the forces generated during the animal's gait and the loads associated with its weight. The tested implants show a higher compressive strength in the longitudinal direction (R_{cw} IS_GR_III = 5 MPa) than in the transverse direction (R_{cp} IS_GR_III = 2.3 MPa), based on which it can be concluded that they can be used successfully in long limb bones, where the dominant amount of load is transferred along the bone. The longitudinal compressive strength values of all tested implant variants are in the range of 1–11 MPa. According to the literature, the compressive strength of cancellous bone is 4–12 MPa [22]. The compressive strength R_c in the longitudinal and transverse directions increased after one month of exposure to Ringer's solution compared to baseline (R_{cw} R1_GR_II = 9 MPa, R_{cp} R1_GR_III = 3.5 MPa). In some cases, in the first phase of degradation, the mechanical properties of the material can be improved by additional cross-linked structures, as confirmed in [23]. A significant decrease in compressive strength (R_{cw} R6_GR_II = 1 MPa, R_{cp} R6_GR_III = 0.03 MPa) was observed for samples subjected to 6-month exposure, indicating progressive degradation of the material. The degradation of PLA during the sixth month of incubation in Ringer's solution is confirmed by the study of Morawska-Chochół et al. [18], during which a change in the pH of the solution and an apparent weight loss of the samples were noted after this period. Our study also found a weight loss in implants exposed to Ringer's solution for six months (R6_gr_IV = 8.062 g), while the weight of implants exposed for three months (R3_gr_IV = 8.216 g) increased concerning the baseline condition (IS_gr_IV = 8.136). The sterilized samples exhibit higher values of compressive strength values in the longitudinal direction (R_{cw} S3_gr_III = 7 MPa) than the baseline condition (R_{cw} S3_gr_III = 5 MPa). In the case of transverse compression, the effect of sterilization on compressive strength (R_{cp}) cannot be determined. During the static longitudinal compression test, the highest value of elastic modulus (E) was characterized by samples after 3 sterilization cycles (R3_gr_II = 585 MPa, R3_ gr_III = 502 MPa, R3_gr_IV = 500 MPa). In a study of the effect of sterilization parameters on the mechanical properties of PLA, the authors also described an increase in the elastic modulus of the samples after sterilization [24]. The lowest elastic modulus is found in samples after 6 months of exposure to Ringer's solution (gr_II = 48 MPa, gr_III = 45 MPa, gr_IV = 48 MPa). Progressive degradation caused the samples to become brittle [29], [30]. According to [10], scaffolds show usefulness in bone surgery if their compression elastic modulus is between 0.4 and 350 MPa. In the case of longitudinal compression, implants in the initial state exceed this limit (about 450 MPa), but the results obtained for transversely compressed specimens fall within the mentioned range. Flexural strength determines the vulnerability of the implant in the event of bending forces acting in the direction perpendicular to it. Such loads can be generated, among other things, because of impact or fall. The flexural strength (R_g) of the specimens after each sterilization cycle was lower than the initial condition (gr_VIII: IS = 775 MPa, S1 = 483 MPa, S2 = 48 MPa, S3 = 178 MPa). A decrease in flexural strength after steam sterilization was also reported by Gogolewski et al. [8]. Microscopic observations and EDS analysis of the surfaces of the implants showed the presence of the elements sodium and chlorine, which resulted from soaking in Ringer's solution. Monthly exposure to Ringer's solution increased the hardness of PLA (74.8 ShA) compared to the baseline (73.4 ShA). In addition, the soaking process increased the degree of surface hydrophilicity. A decrease in surface energy values was also observed (IS_γS = 58.5 mJ/m^2, R1_γS = 51.7 mJ/m^2). Measurement of the pore size and thickness of the print path showed no significant differences in the results, depending on the condition of the implant. Implants in the initial state have an amorphous structure. After the exposure process in Ringer's solution, which caused hydrolytic degradation, a semi-crystalline structure was identified. In addition, a color change in the implants was observed as a consequence of exposure to Ringer's solution. To further identify the effect of the degradability on the strength properties, the implants should be tested after prolonged exposure to Ringer's solution. Measurements of the solution's pH should also be included in the study. The PLA implants described in our study are versatile. They can be used as final products in the cases such as fracture non-union or for bone segment restoration post-tumor

resection. Moreover, these implants can serve as semi-products for further CNC fabrication, offering a customizable solution based on the specific needs of each case. This adaptability extends the potential applications of these implants beyond current offerings in the market. CABIOMEDE 3D-printed PLA implants represent a significant advancement in veterinary orthopedics, offering a biodegradable, customizable and potentially more biocompatible alternative to traditional titanium implants. This innovation addresses specific needs in veterinary medicine, particularly for young and growing animals and in complex surgical procedures.

5. Conclusions

Based on the study, the following conclusions and observations were made:

- the implants have a higher compressive strength in the longitudinal direction than in the transverse direction. This is due to the geometry of the implant and the direction of the applied loads, as well as the orientation of the print;
- hydrolytic degradation initiated by exposure to Ringer's solution resulted in a change in structure from amorphous (IS) to semicrystalline (R6). This indicates partial dissolution of the amorphous phase and thus an increase in the percentage of the crystalline phase, which caused the material to become brittle;
- progressive degradation results in brittle fracture of the material, as can be observed in implants after 6 months of soaking;
- the steam sterilization process increases the elastic modulus of the material and decreases the flexural strength;
- the compressive strength values of PLA implants are similar to the properties of spongy bone.

Acknowledgements

The authors would like to thank CABIOMEDE company for providing the scaffolds for testing.

References

[1] ALIZADEH-OSGOUEI M., LI Y., VAHID A., ATAEE A., WEN C., *Hight strength porous PLA gyroid scaffolds manufactures via fused deposition modeling for tissue-engineering applications*, Smart Mater. Med., 2021, 2, 15–25, DOI: 10.1016/j.smaim.2020.10.003.

[2] BAKHTIARI H., NOURI A., KHAKBIZ M., TOLOUEI-RAD M., *Fatigue behaviour of load-bearing polymeric bone scaffolds: A review*, Acta Biomaterialia, 2023, 172, 16–37, DOI: 10.1016/j.actbio.2023.09.048.

[3] BORDELO J.P.A., DIAS M.I.R., CARDOSO L.M.M.L., REQUICHA J.M.F., VIEGAS C.A.A., BARDET J.F., *A 3D printed model for radiuscurvus surgical treatment planning in a dog*, Pesqui. Vet. Bras., 2018, 38, 1178–1183, DOI: 10.1590/1678-5150-PVB-5209.

[4] BORDONI B., BLACK A.C., VARACALLO M., *Anatomy, Tendons*, [Updated: 2023, Apr. 1], [in:] *StatPearls* [Internet]. Treasure Island (FL): StatPearls Publishing; 2023 Jan-. Available from: https://www.ncbi.nlm.nih.gov/books/NBK513237/

[5] COOLEY D.M., WATERS D.J., *Skeletal neoplasms of small dogs: a retrospective study and literature review*, J. Am. Anim. Hosp. Assoc., 1997, 33, 1, 11–23, DOI: 10.5326/15473317-33-1-11.

[6] DE TORA M.D., BOUDRIEAU R.J., *Complex angular and torsional deformities (Distal femoral malunions): Preoperative planningusing stereolithography and surgical correction with locking plate fixation in four dogs*, Vet. Comp. Orthop. Traumatol., 2016, 29, 416–425, DOI: 10.3415/VCOT-15-08-0145.

[7] GAROT C., BETTEGA G., PICART C., *Additive manufacturing of material scaffolds for bone regeneration: toward application in the clinics*, Adv. Funct. Mater., 31, 5, 2021, 1–30, DOI: 10.1002/adfm.202006967.

[8] GOGOLEWSKI S., MAINIL-VARLET P., *The effect of thermal treatment on sterility, molecular and mechanical properties of various polylactides. I. Poly(L-lactide)*, Biomaterials, 1996, 17, 5, 523–529, DOI: 10.1016/0142-9612(96)82727-x.

[9] GREGOR A., FILOVÁ E., NOVÁK. M., KRONEK J., CHLUP H., BUZGO M., BLAHNOVA V., LUKASOVA V., BARTOS M., NECAS A., HOSEK J., *Designing of PLA scaffolds for bone tissue replacement fabricated by ordinary commercial 3D printer*, J. Biol. Eng., 2017, 11, 31, DOI: 10.1186/s13036-017-0074-3.

[10] GUO Z., YANG C., ZHOU Z., CHEN S., LI F., *Characterization of biodegradable poly (lactic acid) porous scaffolds prepared using selective enzymatic degradation for tissue engineering*, RSC Adv., 7, 2017, 34063–34070, DOI: 10.1039/C7RA03574H.

[11] JANDYAL A., CHATURVEDI I., WAZIR I., RAINA A., UL HAG M.I., *3D printing – A review of processes, materials and applications in industry 4.0*, SUSOC, 2022, 3, 33–42, DOI: 10.1016/j.susoc.2021.09.004.

[12] KOMAR E., WOJNOWSKI T., BALICKI I., *Operative treatment of asynchronous growth of the forearm bone in dogs*, Medycyna Weterynaryjna, 1994, 50, 09, 449–453 (in Polish).

[13] LAM G., KIM S.K., *Three-Dimensional Computer-Assisted Surgical Planning and Use of 3-Dimensional Printing in the Repair ofa Complex Articular Femoral Fracture in a Dog*, Vet. Orthop. Soc., 2019, 32, 12–18, DOI: 10.1055/s-0038-1676062.

[14] LEE H.R., ADAM G.O., YANG D.K., TUNGALAG T., LEE S.J., KIM J.S., KANG H.S., KIM S.J., KIM N.S., *An easy and economicalway to produce a three-dimensional bone phantom in a dog with antebrachial deformities*, Animals, 2020, 10, 1445, DOI: 10.3390/ani10091445.

[15] LONGO F., PENELAS A., GUTBROD A., POZZI A., *Three--dimensional computer-assisted corrective osteotomy with a receiver-specificsurgical guide for an antebrachial limb deformity in two dogs*, Schweiz. Arch. Tierheilkd., 2019, 161, 473–479, DOI: 10.17236/sat00216.

[16] MEMARIAN P., PISHAVAR E., ZANOTTI F., TRENTINI M., COMPONOGARA F., SOLIANI E., GARGIULO P., ISOLA M., ZAVAN B., *Active materials for 3D printing in small animals: Current modalities and future directions for orthopedic appli-*

cations, Int. J. Mol. Sci., 2022, 23 (3), 1–25, DOI: 10.3390/ijms23031045.

[17] MIGDALSKA A., BONECKA J., FRYMUS J., TRĘBACZ P., DEGÓRSKA B., KOWALCZYK P., GALANTY M., STERNA J., *A case report of an open contaminated tibia fracture treatment with external fixator in dog* (in Polish), Życie Weterynaryjne, 2016, 91 (7), 511–515.

[18] MORAWSKA-CHOCHÓŁ A., CHŁOPEK J., DOMALIK P., BOGUŃ M., *New composite materials based on polylactide matrix for intramedullary nails* (in Polish), Engineering of Biomaterials, 2011, 14, 106–108.

[19] OLADAPO B., ZAHEDI S.A., ADEOYE A.O.O., *3D printing of bone scaffolds with hybrid biomaterials*, Comp. B, 2019, 158, 428–436, DOI: 10.1016/j.compositesb.2018.09.065.

[20] PN-EN ISO 178:2011. *Plastics – Determination of flexural properties* (*Tworzywa sztuczne: oznaczanie właściwości przy zginaniu*), 2011.

[21] PN-EN ISO 604:2006. *Plastics – Determination of compressive properties* (*Tworzywa sztuczne: oznaczanie właściwości przy ściskaniu*), 2006.

[22] REZWAN K., CHEN Q.Z., BLAKER J.J., BOCCACCINI A.R., *Biodegradable and bioactive porous polymer/inorganic composite scaffolds for bone tissue engineering*, Biomaterials, 2006, 27, 18, 3413–3431, DOI: 10.1016/j.biomaterials.2006.01.039.

[23] ROJEK M., *Methodology of diagnostic testing of polymeric matrix laminate composite materials* (in Polish), 2011, Accessed: Jan. 25, 2023. [Online]. Available: http://openaccesslibrary.com/vol02/wprowadzenie.pdf

[24] ROZEMA F.R., BOS R.R.M., BOERING G., VAN ASTEN J., NIJENHUIS A.J., PENNINGS J., *The effects of different steam-sterilization programs on material properties of poly(L--lactide)*, J. Appl. Biomater., 1991, 2, 1, 23–28, DOI: 10.1002/jab.770020104.

[25] SAPIERZYŃSKI R., *Osteosarcoma in dogs*, Życie Weterynaryjne, 2017, 92, 08, 562–571 (in Polish).

[26] SAPIERZYŃSKI R., *Neoplasms of the musculoskeletal system in dogs and in cats*. Part II. *Chondrosarcoma, multilobular osteochondrosarcoma and feline osteochondromatosis*, Życie Weterynaryjne, 2005, 80, 10, 633–637 (in Polish).

[27] SCHUSTER A.J., DE ABREU J.L.B., POLA N.M., WITEK L., COELHO P.G., FAOT F., *Histomorphometric analysis of implant osseointegration using hydrophilic implants in diabetic rats*, Clin. Orac. Investig., 2021, 25, 10, 5867–5878, DOI: 10.1007/S00784-021-03892-X.

[28] SIQUEIRA R., FERREIRA A.J., RIZZANTE F.A.P., MOURA G.F., MENDONÇA D.B.S., DE MAGALHÃES D., CIMÕES R., MENDONÇA G., *Hydrophilic titanium surface modulate early stages of osseointegration in osteoporosis*, J. Periodontal Res., 2021, 56, 2, 351–362, DOI: 10.1111/jre.12827.

[29] SPEIGHT J.G., *Monomers, polymers, and plastics*, [in:] *Handbook of Petrochemical Processes*, CRC Press, 2019, 421–466.

[30] STACHUREK I., *Problems with the biodegradation of plastics in the environment*, Zeszyty Naukowe Wyższej Szkoły Zarządzania Ochroną Pracy w Katowicach, 2012, 1, 8, 74–108 (in Polish).

[31] TRĘBACZ P., TRĘBACZ E., STERNA J., *Pathological fracture of the humerus in a dog caused by a simple bone cyst*, Med. Weter., 2015, 71 (7), 458–461 (in Polish).

[32] WANG W., ZHANG B., LI M., LI J., ZHANG C., HAN Y., WANG L., WANG K., ZHOU C., LIU L., FAN Y., ZHANG X., *3D printing pf PLA/n-HA composite scaffolds with customized mechanical properties and biological functions for bone tissue engineering*, Compos. B Eng., 2021, 224, DOI: 10.1016/j.compositesb.2021.109192.

[33] ZWIERUCHO M., STROKOWSKA N., *Most common bone and internal organ injuries caused by road traffic accidents – diagnostic imaging and surgical treatment*, Weterynaria w Praktyce, 2018, 15, 06, 38–50 (in Polish).